Mechanism and Machine Theory 130 (2018) 71–85

Contents lists available at ScienceDirect

Mechanism and Machine Theory

journal homepage: www.elsevier.com/locate/mechmachtheory

Research paper

# Design and evaluation of a torque-controllable knee joint actuator with adjustable series compliance and parallel elasticity

Tomislav Bacek*, Marta Moltedo, Carlos Rodriguez-Guerrero, Joost Geeroms, Bram Vanderborght, Dirk Lefeber

*Robotics and Multibody Mechanics Research Group (R&MM), Vrije Universiteit Brussel and Flanders Make, Pleinlaan 2, Elsene 1050, Belgium*

ARTICLE INFO

*Article history:*
Received 23 May 2018
Revised 15 August 2018
Accepted 16 August 2018
Available online 25 August 2018

*Keywords:*
Compliance
Series elasticity
Parallel elasticity
Variable stiffness
Actuator
Torque controller

ABSTRACT

Compliant actuators are increasingly being designed for wearable robots (WRs) to more adequately address their issues with safety, wearability, and overall system efficiency. The advantages of mechanical compliance are utilized in a new actuator designed to exploit inherent gait dynamics. Unlike any other orthotic power unit, it combines Variable Stiffness Actuator (VSA) and Parallel Elasticity Actuation (PEA) unit into a single modular system. This way, the actuator has the potential to provide the benefits of VSA when net-positive work is necessary and efficiently store energy during energetically conservative tasks. A novel real-time torque controller allows the two units to work together throughout the gait cycle. The design aspects and experimental evaluation of the actuator and its low-level torque controller are presented in this paper. The actuator characterization, carried out in two benchmarking environments, highlights the actuator's high torque density and favorable energetic performance, providing evidence for its applicability in a standalone or multiple-joint lower limb orthoses.



## 1. Introduction

Human walking, as well as other activities of daily life (ADLs), requires a complex interplay between neural and musculoskeletal systems. This interplay, among other things, enables humans to adapt to new situations when confronted with task and/or environmental constraints. To interact with humans in such a constrained daily environment, wearable robots (WRs) need to be flexible, adaptable, and, most importantly, safe. One of the hallmarks for achieving that goal is compliance.

Compliance plays an essential role in human adaptations to external environmental changes and achieving stable gait [1]. Moreover, it has multiple advantages over a traditional stiff actuation [2] used in the field of human-robot interaction. Nevertheless, compliance has not found its way into commercial WRs, which still use direct drive actuation due to its high bandwidth and controllability. A different trend can be seen in research prototypes, where the introduction of an elastic element into a drivetrain led to different realizations and applications of series elastic actuators (SEAs). These include MINDWALKER [3] and IHMC [4] lower body exoskeletons, iT-Knee [5] knee joint orthosis, and stationary gait rehabilitation robots LOPES [6] and ALTACRO [7].

* Corresponding author.
*E-mail address:* tbacek@vub.be (T. Bacek).

https://doi.org/10.1016/j.mechmachtheory.2018.08.014
0094-114X/

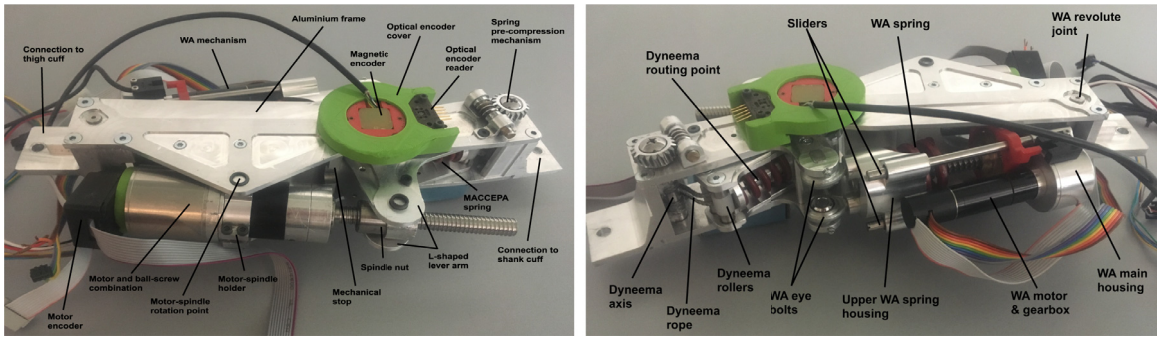


(a) The knee actuator - front side (b) The knee actuator - back side

**Fig. 1.** A modular compliant knee joint actuator consisting of parallel and series elasticity units, thus combining the advantages of both. Parallel elasticity is realized as a quasi-passive mechanism consisting of an EC motor, spindle, and a spring. Series elasticity is realized as a MACCEPA (VSA) due to its simplicity, compactness, robustness, and favorable output characteristic. Such an approach has the potential to lead the actuator to a better energetic performance. The actuator's range of motion is 5° in the extension and 90° in flexion limited by mechanical stops.

In order to overcome their bandwidth limitations and improve their force/torque performance, several modifications have been proposed to traditional SEAs [8,9]. However, the SEAs' energy storage capability and output dynamics depend on the resulting fixed spring constant whose choice remains bound to a certain application/control strategy, severely limiting its applicability. The introduction of VSAs [10] overcame that and enabled the embodiment of characteristics found in biological systems in a new generation of mechatronic systems. Actuation units that exploit variable stiffness include MACCEPA [11], CompAct-VSA [12], AwAS-II [13], ARES [14], and BAFSA [15]. However, despite their indisputable benefits, many VSAs reported in the literature never came to be used in WRs since their energy-saving benefits usually come at the cost of a higher complexity, size, and/or weight. That is not the case with ARES, recently used in ATLAS exoskeleton and the MACCEPA. Ever since its introduction, the MACCEPA concept has been successfully used to develop actuation systems for different applications, including walking exoskeleton [16], stationary gait rehabilitation robot [7], ankle orthosis [17], and ankle-knee prosthesis [18].

Apart from a series compliance unit, WRs can also benefit from a PEA unit. This unit, placed parallel to an actuator's drivetrain/joint, reduces its motor peak torque requirements and, consequently, its power consumption by offloading the motor [19]. Such a configuration is especially useful in a case when a biological joint resembles the behavior of a spring, as is the case with the knee joint's early stance gait phase. Several efforts where this concept was exploited in the knee joint orthoses [20–22] and prostheses [23,24] can be found in the literature. In order to avoid compromising the joint's movement dexterity, all these devices share the employment of a spring (dis)engagement mechanism and a quasi-passive design that exploits mainly elastic, spring-like behavior of the knee joint but has cannot actively input energy into the system.

However, regardless of its realization and adjustability properties, compliance is not sufficient to ensure safe, robust, and biologically relevant actuation in human-robot interaction and needs to be complemented by the appropriate control strategies [25] on two levels. On a low level, the control needs to ensure that a motor reaches any given setpoint to result in a desired user's behavior, previously defined on a high level. As discussed in [26] and [27], low-level controllers used in the literature vary substantially depending on the application and functionality of the actuator. Nevertheless, some trends, dominated by a predefined gait trajectory control [28] and a force/torque control [26] can be identified. The most prominent realizations of both approaches can be found in [29], where the authors compared a torque-tracking performance of different torque controllers under realistic experimental conditions. However, despite such efforts, it is not clear which, if any, combination of a high- and low-level controller is the optimal in any given scenario.

All these WRs' components discussed above are embodied in the actuator presented herein in detail (see Fig. 1), designed as a research platform to investigate the effects of its varying output stiffness on the users' biomechanics and energetic performance across and not within different daily activities. This is made possible by introducing the following novelties:

1. Its overall design is guided by a modularity requirement, leading to an actuator that can be used as a standalone or part of a multiple-joint lower limb orthosis. This modularity also allows the actuator to be used in different assistive and structural configurations (passive degrees of freedom), thus analyzing the effects these have on both the actuator and the user.
2. It utilizes a spindle-driven MACCEPA concept realization tailored for use in a human knee joint orthosis. The simplicity and controllability of the MACCEPA concept are combined with wearability and safety requirements to deliver a compact and a high-power actuator with desirable inertia distribution and the potential for increased energetic efficiency.
3. Its non-linear output characteristic is exploited to devise a robust low-level controller in analytic form, allowing joint stiffness and torque control to be realized in real-time. In addition, this controller can be used with other realizations of the MACCEPA concept.

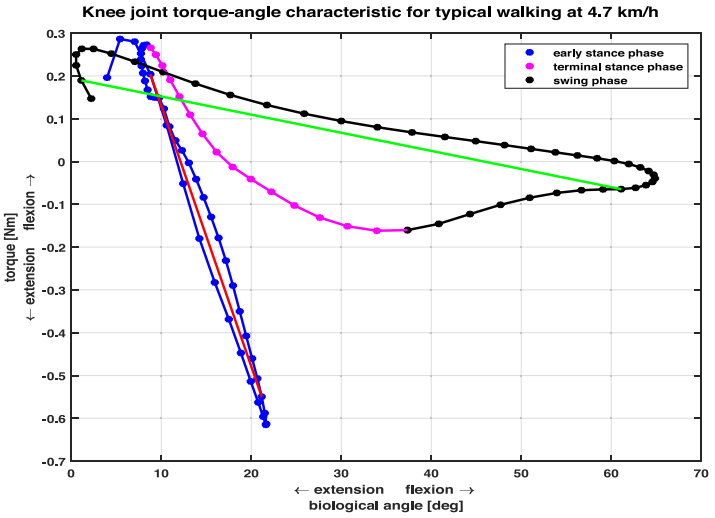


**Fig. 2.** The knee joint torque-angle characteristic of a typical healthy person during walking [33]. Qualitatively similar characteristics also hold for slower and faster walking [33,34]. The gait starts with a heel strike and ends with the subsequent heel strike from the same leg. The early stance phase can be approximated by a stiff spring whose stiffness equals the red line slope and the late stance and swing phase can be approximated by a compliant spring whose stiffness equals the green line slope. This clear division is exploited in the actuator's design, which employs two springs. (For interpretation of the references to color in this figure legend, the reader is referred to the web version of this article.)

4. It combines series and parallel elasticity units into a single orthotic actuator to fully mimic the dynamic behavior of the knee joint during gait. To the best of our knowledge, this is the first such device to be used in orthotics. Consisting of two independent yet complementary subsystems, this actuator takes advantages of both concepts in order to deliver biologically relevant behavior while exploiting natural dynamics of the task. It has the potential to provide the benefits of a VSA during energetically non-conservative tasks, when net-positive work is necessary, and efficiently store energy during cyclic, energetically conservative tasks. Moreover, it has the potential to combine its dual compliance to extend the range of its attainable output impedances during certain ADLs.

The work presented herein builds upon our work previously presented at the 2017 IEEE IROS conference in Vancouver, Canada [30]. The contributions of this paper include a detailed mechanical design of the whole actuator and a numerical optimization leading to it, a real-time low-level MACCEPA torque controller, a presentation of a dynamic benchmarking environment and an extensive static and dynamic tests results that include a joint operation of the MACCEPA and the WA mechanism.

The remainder of the paper is organized as follows. A discussion on how a human knee joint biomechanics is exploited in the actuator's design is given in Section II. In Section III, conceptual and actual realizations of the presented knee joint actuator are presented in detail, followed by a newly developed low-level torque controller description in Section IV. Section V gives an overview of the test setup used to assess the actuator's behavior in two different benchmark environments (quasi-static and dynamic), while Section VI gives results of the extensive actuator benchmarking in an experimental test setup. The final section of the paper contains discussion, conclusions, and the scope for future work.

## 2. Knee joint biomechanics

A knee joint has a complex anatomy that allows it a wide range of roles in ADLs, but it also makes it hard to mimic [31]. As the most exercised daily activity, walking is used as a guideline in the presented actuator's design. The actuator is, however, designed to be operable in other ADLs as well. While walking, a knee joint is responsible for shock absorption at the moment of heel strike, body weight support during the early stance phase, stability during the terminal stance phase, and leg flexion during the swing phase, thus assisting foot clearance. These different gait phases can be seen in Fig. 2. The early stance phase, also known as the weight acceptance (WA) phase (blue circles), takes up approximately 40% of a gait cycle, while the terminal stance phase (purple circles) takes up approximately 23% [21]. During the flexion and extension stages of the early stance phase, a knee joint exhibits similar stiffness, the smallest difference occuring at a preferred gait speed [32]. This implies that a knee joint behaves similar to a linear torsional spring in this phase.

Humans tend to regulate their lower limb biomechanics so as to preserve the knee joint's overall linear behavior during the WA phase [35], which can be represented by a slope of the best linear fit on the joint's torque-angle characteristic (red curve of slope $\kappa_{QS}$ in Fig. 2). This slope is known as quasi-stiffness. Implementing a spring parallel to the actuator's joint so that the resulting angular stiffness corresponds to $\kappa_{QS}$ would allow energy savings while achieving the best torque tracking during walking [36]. If implemented in a quasi-passive device, a good torque-angle approximation can be achieved while keeping the actuator's energy consumption to a minimum [19].

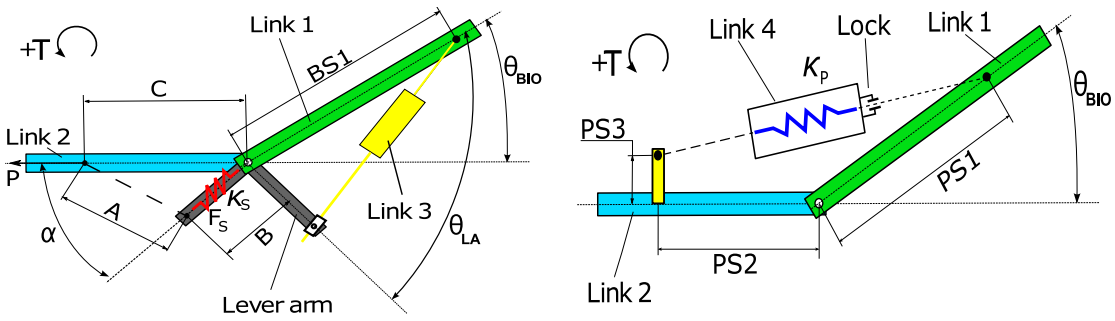


(a) Schematic design of the MACCEPA. (b) Schematic design of the WA mechanism.

**Fig. 3.** Schematic design of the presented knee joint actuator. *Link 1* (input link, green) and *Link 2* (output link, light blue) are structural links shared by both series and parallel elasticity units. a) A spindle-driven MACCEPA concept realization, consisting of an L-shaped lever arm (in grey) with a spring (in red) and a ball-screw spindle drive (*Link 3*). The deflection angle $\alpha$ is controlled via a ball screw drive by controlling the lever arm angle $\theta_{LA}$. A detailed description of the MACCEPA parameters and working principle can be found in [37]. b) A spring mechanism parallel to the actuator joint. The mechanism (*Link 4*) spans the joint without obstructing its range of motion. The torque coming from the mechanism when engaged by the *Lock* depends on the stiffness of a spring (in blue) and its effective length. The stiffness $\kappa_P$ is fixed. (For interpretation of the references to color in this figure legend, the reader is referred to the web version of this article.)

High stiffness of the early stance phase is not preserved across a gait cycle, suggesting the need for the implementation of a compliant spring for the remainder of the cycle as part of either a passive or an active device [23]. Implementing it in an active device ensures the ability to accurately deliver the torque-angle characteristic of the terminal stance phase and the swing phase by actively injecting/dissipating energy into/from the system.

## 3. Mechanical design

### 3.1. Series and parallel elasticity concepts

A series elasticity unit has the potential to improve an actuator's mechanical energy utilization by decreasing its motor velocity [19]. The presented knee joint actuator employs series elasticity by utilizing the MACCEPA concept [11] (Fig. 3a). The MACCEPA is a torque-controlled VSA concept that works as a torsion spring allowing independent control of its equilibrium position and output stiffness. In short, a MACCEPA-based actuator works by creating a force $F_S$ in a spring in series with the motor coming from the controlled *Lever arm* deflection angle $\alpha$. The resulting joint torque $T$ coming from this spring compression tends to re-align the output link (*Link 2*) and the lever arm, thus bringing the output link into a new equilibrium position (defined by the biological angle $\theta_{BIO}$ between the *Link 2* and *Link 1*). Bidirectional motion of the lever arm allows a MACCEPA-based actuator to exert both positive and negative torques around the joint axis.

The MACCEPA theoretical model output is given by:

$$\tau_{macc} = \kappa_S \cdot B \cdot C \cdot \sin(\alpha) \cdot \left(1 + \frac{P - |C - B|}{A}\right), \tag{1}$$

where $\kappa_S$ and $P$ denote the MACCEPA's spring stiffness and pre-compression, respectively, while $A$, $B$ and $C$ are its geometric parameters (see Fig. 3a). Any change in the spring pre-compression $P$ effectively changes a MACCEPA-based actuator's angular stiffness, as seen in the joint. The presented actuator can only change its apparent stiffness offline, i.e. across multiple gait cycles/activities, as opposed to an online stiffness change within a single gait cycle (see [14]). As it was designed as a research platform, this *constraint* does not prevent the presented actuator from being used to examine the effects its varying output impedance has on the biomechanics and the energetic expense of users walking in controlled testing environments.

A PEA unit also has the potential to improve an actuator's energy efficiency during cyclic motions by decreasing its motor torque requirements [19]. To do so, the presented actuator uses a quasi-passive PEA unit (WA mechanism, as given in Fig. 3b), to store and release the energy coming from changes in gravitational potential energy during the early stance phase. Being connected to both sides of the actuator's joint, the PEA unit would obstruct a knee joint's flexion if no spring disengagement mechanism was employed. Hence, the presented actuator exploits a friction-based locking during the early stance phase to passively store the available energy in the spring. After the loading phase ends, the spring is disengaged by means of a small motor, thus allowing the joint to freely move during the swing phase and other ADLs.

In the application scenario, during walking, the two actuation units can work in concert at least in two different ways. Assuming a reference torque is known from a high-level controller and that the system is aware of the gait cycle phase it is in (by using foot-switches), the MACCEPA can either be *silent* during the early stance phase or can superimpose the WA mechanism. In the former case, it is assumed that the WA spring is optimized for a given gait scenario and can provide the required torque, allowing the MACCEPA to be in a zero-torque mode. In the latter case, the required early stance phase

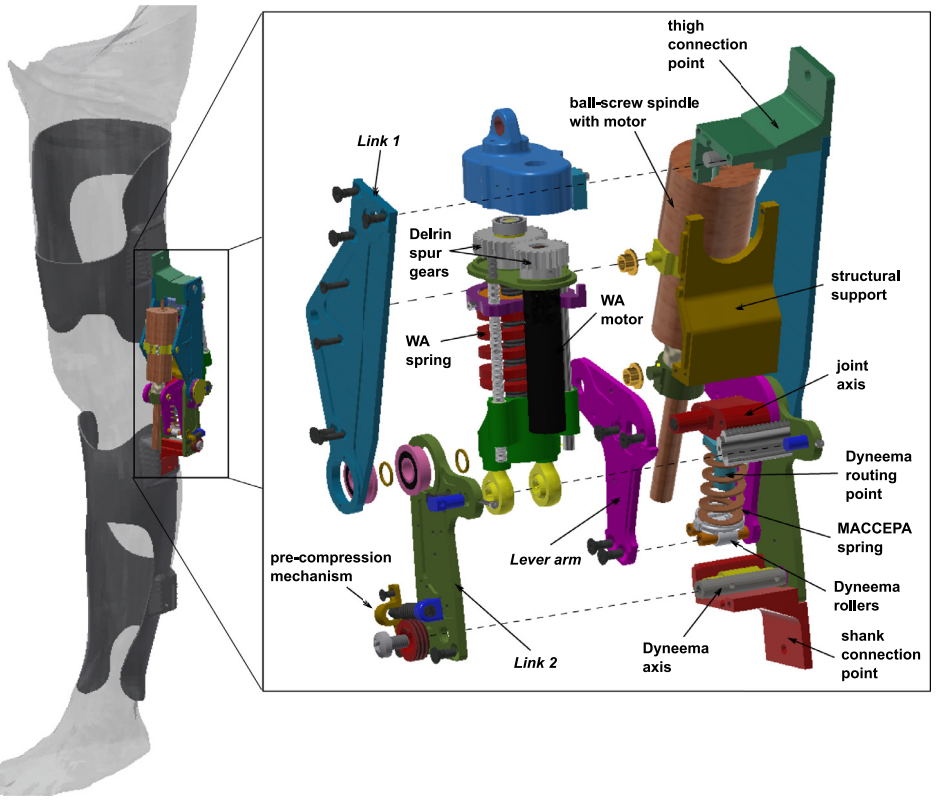


**Fig. 4.** A CAD model of the actuator. On the left, the intended fixation of the actuator to the in-house built personalized orthosis [42] is depicted. A zoomed-in window (on the right) shows an exploded view of the actuator.

torque cannot be satisfactorily delivered by the WA mechanism due to its sub-optimal spring, requiring the MACCEPA to superimpose the WA mechanism and correct the actuator's output torque. The sensors implemented in the actuator allow accurate torque output estimation of each of the two units, allowing online torque correction, should that be necessary. Furthermore, the superimposing mode has the potential to overcome the main WA mechanism's drawback - a constant angular stiffness - by combining outputs from both actuation units.

### *3.2. Actual realization of the actuator*

The presented actuator exploits a distinctive feature of a knee joint's gait kinematics and kinetics by employing the springs working both in series and in parallel to the actuator's joint. In practice, this led to an actuator to consist of two independent yet complementary actuation units, each employing one of the two springs. Although independent, the two units share their main structure (*Link 1* and *Link 2*, as shown in Figs. 3 and 4). The main structure is guided by an anthropomorphic design approach, modularity, and the sagittal-plane-only torque delivery requirement. A revolute-joint actuator is chosen for simplicity and compactness and is supported by several works, showing that such a simplification of a biological knee joint is a viable choice for the range of motion experienced during walking [21,38,39]. Moreover, such a configuration will allow the future testing of the effects of adding auxiliary passive joints [40,41] on the user's biomechanics and energy expenditure.

In the application scenario, when fitted to a knee joint orthosis, the *Link 1* is intended to be placed along the thigh and the *Link 2* along the user's shank (see Fig. 4), thus reducing the actuator's inertial effects on the total below-knee inertia. Decreased lateral protrusion and improved mass and inertia distribution are achieved by realizing the MACCEPA around a highly efficient, backdrivable ball-screw spindle and the WA mechanism around a non-backdrivable trapezoidal spindle. Due to their multiple advantages, spindles have been increasingly used in orthotic [3,14,20,43] and prosthetic [23,24] prototypes. The downside of using a spindle directly connected to a lever arm, as is the case with the MACCEPA, is a limited range of motion and a nonlinear mechanical advantage, inversely proportional to the knee joint's flexion angle.

The MACCEPA motor-spindle combination is fixed to the *Link 1* by means of two rotational joints. By implementing a similar connection to the lever arm, the ball-screw spindle is allowed to self-align throughout the whole range of motion, thus avoiding radial forces from acting on it. The lever arm, shaped in the form of an *L*, is placed within the *Link 2* together with the spring (in series to the MACCEPA motor) and the pre-compression mechanism. By placing the spring in between

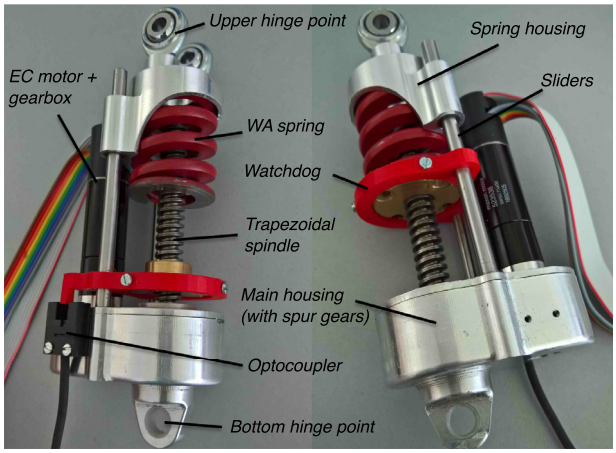


**Fig. 5.** The WA mechanism depicted in a disengaged (left) and an engaged (right) position. The optical switch is used to home the spring and initialize motor encoder. To connect the output of the motor with the spindle, a gearbox and a set of spur gears are used. The motor, transmission and the spindle are all fixed to the mechanism's main housing. Similar realization of the WA mechanism can be found in [23].

the lever arm's structural aluminum plates, the actuator size and weight was reduced. To create a force in the spring during the controlled lever arm deflection, a very strong, robust, and durable $\phi$2mm Dyneema® rope with a favorable stretching characteristic is used (Fig. 1). By wrapping the rope around *Dyneema axis* using a simple keyed worm-gear system, guiding it between *Dyneema rollers*, and routing back through *Dyneema routing point* (Figs. 1 and 4), the actuator's spring pre-compression can be easily changed, effectively changing its output impedance. In order to be fully controllable, the MACCEPA uses a 5V 14-bit absolute magnetic encoder AS5048A to measure the lever arm angle $\theta_{LA}$ and a 5V incremental optical encoder US Digital HUBDISK-2-2000-625-IE and an accompanying module EM1-2-2000-I to measure the biological angle $\theta_{BIO}$ (see Fig. 3)

In order to get the MACCEPA's design and drivetrain parameters, a constrained minimization was carried out in Matlab® defined as follows:

$$\begin{aligned} \underset{\hat{\mathbf{x}}}{\text{minimize}} \quad & \int_0^{T_{gc}} P_{mech}\, dt \\ \text{subject to} \quad & \mathbf{x}_{min} \le \hat{\mathbf{x}} \le \mathbf{x}_{max} \\ & \hat{B} + L_0 \le \hat{C} \\ & ||\hat{\mathbf{T}}_{macc} + \hat{\mathbf{T}}_{WA} - \hat{\mathbf{T}}_{bio}||_2 \le \delta_T \end{aligned} \tag{2}$$

where $T_{gc}$ denotes a gait cycle duration, $P_{mech}$ denotes the actuator's mechanical power on the spindle nut, $\hat{\mathbf{x}} = [\hat{\theta}_{LA}\ \hat{\kappa}_S\ \hat{P}\ \hat{B}\ \hat{C}\ \hat{B}_{S1}]$ an optimization vector, and $L_0$ the minimum distance between the MACCEPA parameters $B$ and $C$. $\hat{\mathbf{T}}_{macc}$, $\hat{\mathbf{T}}_{WA}$ and $\hat{\mathbf{T}}_{bio}$ are the MACCEPA, the WA mechanism, and the biological gait reference torque, respectively, while $\delta_T$ is a torque error upper boundary. According to the work by Verstraten [44], minimizing the mechanical energy consumption is a viable drivetrain parameter selection method.

The goal of the parameter search was to deliver a scaled knee joint torque-angle characteristic (peak 50Nm) during normal and slow gait as given in [33]. In simulations, the MACCEPA was not working during the early stance phase since this phase's torque ($\mathbf{T}_{WA}$) was delivered by the WA mechanism. As a result of the minimization and available components on the market, the presented MACCEPA was initially powered by a Maxon EC-i40 50W motor (36V). However, this motor was replaced during preliminary tests by a more powerful, 70W version, as the latter was only slightly heavier but capable of delivering higher torques needed in other ADLs when the WA mechanism is not used. The motor is coupled with a Maxon GP32S ball-screw spindle drive ($10 \times 2$, gearbox 3.7:1) and Sodeman ISO die compressive spring of effective stiffness $\kappa_S =$ 183.3 N/mm, chosen as a series elasticity spring. Despite high transmission coming from the spindle, the 3.7:1 gearbox is used to further increase the maximum output torque while minimally compromising backdrivability (and because this is the smallest gearbox ratio available from the manufacturer besides 1:1). However, the gearbox also decreases the actuator's maximum attainable velocity. This is because the higher total transmission ratio pushes the required motor velocities needed to deliver a gait cycle outside the manufacturer's rated operating values. To keep the motor velocities within manufacturer-specified range, slower-than-normal (4.7 km/h according to Winter data [33]) gait velocities can be attained.

Another actuation unit employed in the actuator is the WA mechanism (Fig. 5), a quasi-passive device used to (dis)engage the WA spring and exploit a spring-like behaviour of the knee joint's early stance gait phase. The mechanism spans the actuator's joint, directly attaching to the *Link 1* and *Link 2* (see Figs. 3b and 4), but unlike the MACCEPA, it has the motor installed parallel to the spindle. The main housing is attached to the *Link 1* via a revolute joint. The connection to the *Link 2* is done via two eye bolts fixed to the spring housing, which slides over the slides fixed to the main housing. Such a

configuration ensures the WA mechanism's self-alignment in the whole knee joint's ROM, avoiding radial loading on the spindle and allowing unobstructed knee motion.

In order to get the WA mechanism's design and drivetrain parameters, a constrained minimization was carried out in Matlab® defined as follows:

$$\begin{aligned} \underset{\hat{\mathbf{y}}}{\text{minimize}} \quad & \|\hat{\mathbf{T}}_{WA} - \hat{\mathbf{T}}_{bio,ES}\|_2 \\ \text{subject to} \quad & \mathbf{y}_{min} \leq \hat{\mathbf{y}} \leq \mathbf{y}_{max} \end{aligned} \tag{3}$$

where $\hat{\mathbf{y}} = [\hat{\kappa}_P \; \hat{PS}_1 \; \hat{PS}_2 \; \hat{PS}_3]$ is an optimization vector and $\hat{\mathbf{T}}_{bio,ES}$ is the biological joint torque during the early stance phase (see Fig. 3b for details on the mechanism's geometric parameters).

As a result of the minimization and available components on the market, the WA mechanism uses Sodeman die compressive spring of effective stiffness $\kappa_P = 225$ N/mm and a Schiltz trapezoidal spindle ($10 \times 3$) with a bronze nut. The total transmission ratio of 10.5 between the spindle and the Maxon EC16 30 W (36 V) motor is achieved through Delrin spur gears (35:18 gear ratio) and a Maxon planetary gearhead GP16C (ratio 5.4:1). The spring is glued to the spring housing to reduce the mass and inertia of the movable parts that motor needs to operate. Consequently, the motor's power consumption can be reduced. The spindle is non-backdrivable to offload the motor during the gait's loading phase. Another advantage of this system is the possibility to be engaged at any desired knee joint flexion angle (i.e. the mechanism has an infinite engagement angle), which varies for each subject depending on their mass, walking velocity, and walking pattern [32].

The WA mechanism works as follows. When the system power is on, the nut is initialized by moving to its resting position (proximal to the main housing) until the optocoupler's signal is detected. During the swing phase, the nut is moved up along the spindle to be at the engaging position at the time of a heel strike. During the WA phase and spring loading, the motor is switched off since the reactionary torque is provided by friction-locking the nut (overview of different locking mechanism is given in [23]). Once the unloading is finished, the nut moves back to its disengaged position (proximal to the main housing), allowing unobstructed knee motion. During other ADLs, the nut can be kept in this position, but it can also be used to prevent the person from falling by actively moving with the knee. In the current design, the nut cannot be moved during the loading phase.

## 4. Low-level control

### 4.1. MACCEPA torque controller

One of the main advantages of compliant actuators is their intrinsic property of turning a force/torque control problem into a position control problem [2], which is easier to realize. Usually, a force/torque is a linear function of a linear/angular spring displacement leading to a straightforward application of the Hooke's law. The same does not hold in the MACCEPA case as both its output torque and apparent stiffness are generally a nonlinear function of the spring pre-compression $P$ and deflection angle $\alpha$. For this reason, a low-level MACCEPA torque controller can be theoretically described using the following equation:

$$\tau_{joint}^{ref} = \hat{\kappa}_{joint}(\alpha) \cdot f(\alpha_{ref}), \tag{4}$$

where $\tau_{joint}^{ref}$ is the reference torque coming from a high-level controller, $\hat{\kappa}_{joint}(\alpha)$ is the estimated torsional (angular) joint stiffness, and $f(\alpha_{ref})$ refers to some nonlinear function of the deflection angle. Thus, the control strategy presented in this paper aims at delivering the desired joint torque in an open loop by controlling the deflection angle $\alpha$ in an inner loop (cascaded control) while estimating torsional joint stiffness $\hat{\kappa}_{joint}$ in the actuator's torque-stiffness workspace.

The control law in Eq. (4) is based on experimental data as the function $f(\alpha)$ depends on the actuator's mechanical realization. The experiments to obtain $f(\alpha)$ were carried out using a simple closed-loop torque controller (different from the open loop torque controller mentioned above) in a quasi-static test setup (see Section V). In short, the actuator's *Link 1* and *Link 2* (Fig. 3) were fixed in the test setup with a torque sensor measuring the output torque, making the lever arm the only movable link. The sinusoidal torque setpoint was imposed on a simple $P$ torque controller with the torque feedback coming from a torque sensor. Experiments were repeated for different spring pre-compressions with the motor velocity control implemented as an inner control loop.

The outcome of these experiments gives the actuator's torque-angle characteristic for each tested spring pre-compression (see Fig. 6a). As the characteristics exhibit hysteresis, a third order polynomial $\tau_{approx}$ approximating each characteristic is used in further calculations (Fig. 6a). Assuming that the torque approximation is a piece-wise linear function, the linear Hooke's law $\tau = \kappa \cdot \alpha$ holds in a small neighborhood of each data-point. Consequently, a related quasi-stiffness characteristics $\kappa_{approx}$ can be approximated using a second order polynomial (Fig. 6b), obtained as $\kappa_{approx} = \frac{\partial \tau_{approx}}{\partial \alpha}$. Once these approximations for each different pre-compression are known, the experimental values of the function $f(\alpha)$ from Eq. (4) can be obtained as follows:

$$f_i(\alpha) = \frac{\tau_{i,approx}}{\kappa_{i,approx}}, \tag{5}$$

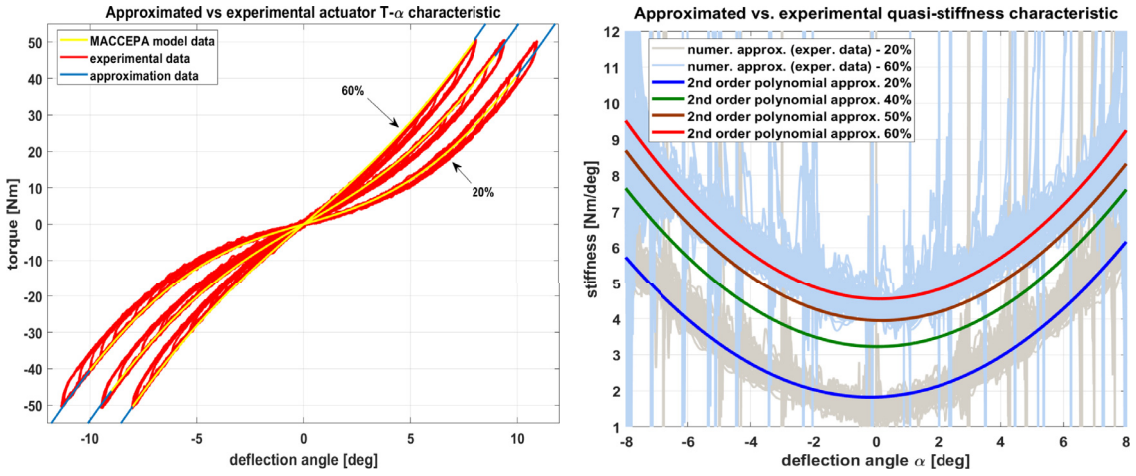


(a) MACCEPA's torque-angle characteristics. (b) MACCEPA's projected stiffness.

**Fig. 6.** MACCEPA torque and stiffness characteristics. a) The torque-angle characteristics for 20%, 40%, and 60% spring pre-compressions. Each experimental characteristic (in red) contains data from different-amplitude sinusoidal reference trajectories. Due to an existing hysteresis, experimentally obtained characteristics are approximated by a third order polynomial (in blue) used in calculations, which matches well with the MACCEPA model output (in yellow). b) The stiffness-angle characteristics for different pre-compressions. The experimental characteristics (shown only for 20% and 60% pre-compression) are obtained as a numerical derivative of the experimental torque data (spikes come from numerical errors). The second order polynomial approximating experimental stiffness characteristics accurately follow the trend of the quasi-stiffness change. The actuator has an output stiffness range from 0 to 8.5 Nm/deg (487 Nm/rad) at $\approx 0°$ deflection angle $\alpha$, i.e. not considering the stiffening effect (a positive correlation between the torsional joint stiffness $\kappa$ and an absolute value of the deflection angle $\alpha$). The maximum value of 8.5 Nm/deg is obtained from a model and corresponds to a stiffness at the maximum 100% spring pre-compression. (For interpretation of the references to color in this figure legend, the reader is referred to the web version of this article.)

where index $i$ corresponds to the spring pre-compressions of 20–60% in increments of 10. This function can be approximated by the hyperbolic tangent function of the following form:

$$f_i(\alpha) \approx G_i \cdot \left( \frac{2}{e^{-\mu_i \cdot \alpha} + 1} - 1 \right), \tag{6}$$

where coefficients $G$ and $\mu$ correspond to the amplitude and slope of the $f(\alpha)$ function, respectively. Since $f_i(\alpha)$ is known from the experiments (see Eq. (5)), it is easy to find coefficients $G_i$ and $\mu_i$ by simply performing numerical fitting for a range of deflection angles $\alpha$. Subsequently, once the coefficients for each pre-compression are known, polynomials $G(P)$ and $\mu(P)$ of the $n$th order that estimate these coefficients for any pre-compression level in the 0–100% range can be found.

As mentioned earlier, a simple closed-loop torque controller was used during the experiments carried out to obtain the actuator's torque-angle characteristics. All other tests were carried out using an open loop torque controller in series with a closed loop position controller, in which the deflection angle $\alpha$ is the actual control variable. Hence, it is useful to rewrite the Eq. (6) as:

$$\alpha_{ref} = -\frac{1}{\mu(P)} \log_e \left( \frac{2}{\frac{f(\alpha_{ref})}{G(P)} + 1} - 1 \right), \tag{7}$$

with condition $-1 < \dfrac{f(\alpha_{ref})}{G} < 1$ coming from the requirement that the logarithmic function in Eq. (7) attains a real solution. However, as the function $f(\alpha)$ in the Eq. (6) is calculated from the experimental data, this condition is always satisfied.

The only unknown coefficient in the above equation, given the pre-compression $P$, is the value of the function $f(\alpha_{ref})$, which can be obtained from the Eq. (4). When Eq. (4) is substituted by the Eq. (7), the reference deflection angle $\alpha_{ref}$ becomes:

$$\alpha_{ref} = -\frac{1}{\mu(P)} \log_e \left( \frac{2 \cdot \hat{\kappa}_{joint} \cdot G(P)}{\tau_{joint}^{ref} + \hat{\kappa}_{joint} \cdot G(P)} - 1 \right). \tag{8}$$

For any given reference torque $\tau_{joint}^{ref}$ coming from a high level controller and any given spring pre-compression $P$ preset offline, the low-level MACCEPA torque controller estimates joint stiffness $\hat{\kappa}_{joint}$ and calculates the reference deflection angle $\alpha_{ref}$ online in real time. This allows the actuator to respond to any torque reference within its software and hardware safety limitations without any additional modifications. Furthermore, this controller can be used unmodified with MACCEPA realizations that can change pre-compression online, thus allowing a simple implementation of a real-time joint stiffness

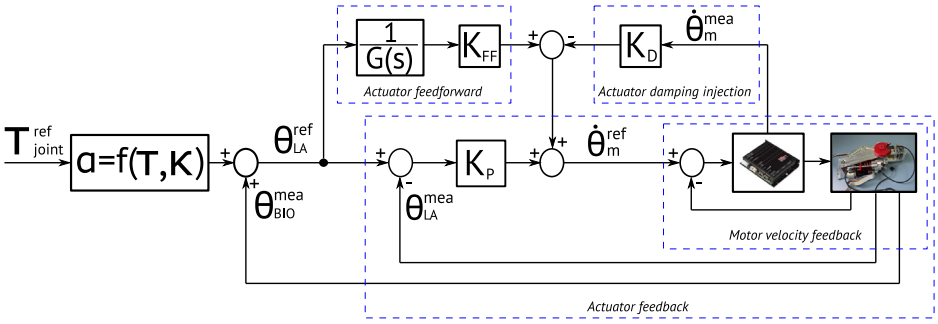


**Fig. 7.** Block diagram of the low-level MACCEPA torque controller. Based on the measured biological joint angle $\theta_{BIO}^{mea}$ and the reference deflection angle $\alpha_{ref}$ calculated online from the Eq. (8), the reference lever arm angle $\theta_{LA}^{ref}$ is calculated. The lever arm angle is then fed into both feedback (FB) and feed-forward (FF) branches of the controller. To improve the actuator's response, the measured motor velocity $\dot{\theta}_m^{mea}$ is multiplied by a damping factor $K_D$ and added to the motor velocity setpoint coming from the FB and FF branches. The *G(s)* in the FF branch is a simple geometric expression relating the MACCEPA's motor velocity to its lever arm angular position.

control. While such an online joint stiffness control requires a separate control law, the actual joint stiffness coming from this law can be inserted into the Eq. (8) as $\hat{\kappa}_{joint}$, allowing the controlled changes in the joint stiffness to continuously be taken into account.

Fig. 7 shows the low-level MACCEPA torque controller block diagram. Similar to the most prominent controller in [29], the presented controller employs a simple proportional feedback control on deflection angle with a damping injection on measured motor velocity. However, instead of using iterative learning branch, the presented controller uses the feed-forward (FF) branch scaled by the factor $K_{FF} \leq 1$. The FF branch uses the knowledge of the MACCEPA's geometry and current configuration to predict the motor velocity signal needed to produce an ideal response. This branch was added only during dynamic testing (see Section V), when the *Link 2* (Fig. 3) is moving once it became clear that the feedback (FB) alone could not cope with the actuator's non-linearities. The FB branch is now only required to provide corrections and respond to disturbances, potentially increasing the actuator's bandwidth.

### *4.2. Weight-acceptance mechanism position control*

As a quasi-static actuation unit, the WA mechanism's low-level control is implemented as a simple nut position control. The mechanism needs to move the trapezoidal spindle nut to one of the two extreme positions (see Fig. 5): engagement position (high) or disengagement position (low). When disengaged, the nut is in the lowest position on the spindle, thus allowing the knee to flex up to 90° (mechanical limit). The signal from the optocoupler is used to indicate when the lowest position has been reached. On the other hand, the nut's position along the spindle, when engaged, depends on the desired torque-angle response during the WA phase. Each position of the nut along the spindle corresponds to a different engagement angle, resulting in a theoretically infinite engagement resolution of the presented WA mechanism. When the desired engagement angle is known, the error between the setpoint and actual motor position is calculated and fed into a simple *P* controller. In the inner control loop, the motor is controlled in velocity mode.

## 5. Experimental test setup

The test setup built for both quasi-static (*Link 2* fixed) and dynamic (*Link 2* moving) actuator benchmarking is depicted in Fig. 8. The setup consists of a robust aluminum cage, DRBK torque sensor (200 Nm, ±5 V) with BKE flexible metal bellow couplings from ETH Messtechnik, Beckhoff AM8032 3-phase synchronous servomotor (400–480VAC, OCT with 40:1 NP035S planetary gearbox) powered by Beckhoff AX5203 digital compact servo drive (with EtherCAT), and an actuator fixation points to the cage frame. The three actuator fixation points provide a stiffer connection to the global system when compared to an actual application scenario (when worn by human). The benefit of such a controlled experimental environment is its ability to test the actuator's structural stability and its peak torque performance when operating at its hardware and software-set limits.

In order to allow different types of actuator benchmarking, the setup can be used in at least two different configurations. In the quasi-static configuration, the upper flexible coupling is fixed to the cage frame while the lower is fixed to the actuator's output link, thus preventing the *Link 2* from moving. By making the lever arm the only movable link, it is not possible to emulate a biological torque-angle profile. However, this configuration is useful to carry out experiments needed to characterize the actuator's behavior, such as its stiffness range, output (non)linearity, model validity, and frequency response. In the dynamic configuration, the upper flexible coupling is fixed to the load motor's output axis while the lower is fixed to the actuator's *Link 2*. Such a fixation allows a controlled motion of the actuator's output link by means of a load motor, which is necessary to replicate a biological knee joint angle profile. In addition, this configuration allows testing the actuator's performance using more elaborate control techniques and more realistic actual-application scenarios.

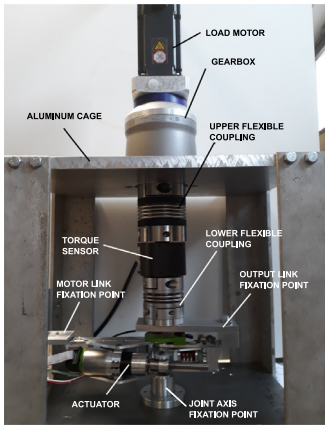


**Fig. 8.** The benchmarking test setup consists of an aluminum cage as its main structural part, a load motor with gearbox to emulate biological angle patterns, a torque sensor with two flexible couplings to account for any misalignments, and three connection points for fixation of the actuator to the cage frame.

Despite their different hardware configurations, both quasi-static and dynamic tests were carried out in the same software environment. The model of the entire setup, including the actuator, sensorics, load motor, and the torque sensor was created in the Matlab Simulink® environment. The real-time communication between PC and all I/O devices (including the Maxon EPOS 70/10 and ESCON 50/5 motor drives) is achieved using the EtherCAT protocol, which employs a master/slave principle. The Beckhoff TwinCAT master environment was used to make a link to the PC's kernel space and turn it into a real-time target that ran and maintained an EtherCAT network at 1KHz. More information on how to set-up such a control environment can be found in [45].

## 6. Results

### 6.1. Quasi-static benchmarking

During the actuator's quasi-static benchmarking, when its output link was blocked, all the tests except the validation ones were carried out using a closed-loop torque controller as explained earlier. This low-level torque controller consisted only of a torque feedback branch, which proved to be sufficient to deliver desired behavior when the *Link 2* was fixed. Since the actuator's output link was blocked, these tests only characterized the MACCEPA unit.

The nonlinearity in the MACCEPA's output torque, as discussed earlier, is clearly present in both the theoretical MACCEPA model and the actual actuator, as Fig. 6a clearly shows. Such a nonlinear behavior, accompanied by the actual measurements' hysteresis, led to a third order approximation of the torque-angle relationship (Fig. 6a) and a second order approximation of the stiffness-angle relationship (Fig. 6b). As no torque sensor will be available in the actual application scenario, it is important that these approximations are accurate and reliable.

Fig. 9a shows the MACCEPA's output torque response to a multi-sine reference torque trajectory, validating the approximations discussed above. Given that this was a controller-validation test, an open-loop torque controller with an inner-loop lever arm position control was used. In other words, a multi-sine torque reference was used to generate the reference lever arm position online ($\theta_{LA}^{ref}$, see Fig. 7), while the measured torque was used in post-processing to compare the reference to the actual output. A multi-sine data was also used to characterize the actuator's bandwidth. As argued in [46], an actuator's torque bandwidth is not a number but a graph reflecting its behavior for general desired torque amplitudes or varying load impedance. To get a good characterization of the actuator's torque bandwidth, a series of tests were carried out using multi-sine torque reference as an input while the actuator's output link was fixed. The load dynamics was not considered in the bandwidth calculations since adding this parameter increases the problem's dimensionality to a level that is out of the scope of this paper. The parameters that were varied during these tests include the reference signal's peak torque amplitude and frequency spectrum, the MACCEPA's spring pre-compression, and the actuator's output link angle ($\theta_{BIO}$ in Fig. 3).

Fig. 9b shows the MACCEPA's bandwidth as a function of a torque and the MACCEPA's spring pre-compression for a fixed angle $\theta_{BIO}$=40°. The graph clearly shows that the actuator's bandwidth can significantly vary, going anywhere from 3.5 Hz at 20% spring pre-compression and high torque to 9.5 Hz at 60% spring pre-compression and low torque. The numbers are slightly different, but of the same order of magnitude for the other two sets of tests ($\theta_{BIO}$=20° and $\theta_{BIO}$=60°). Arguably, the feed-forward controller branch would have led to a higher bandwidth. Being controller-dependent, the reported bandwidth is not necessarily the actuator's physical upper bound.

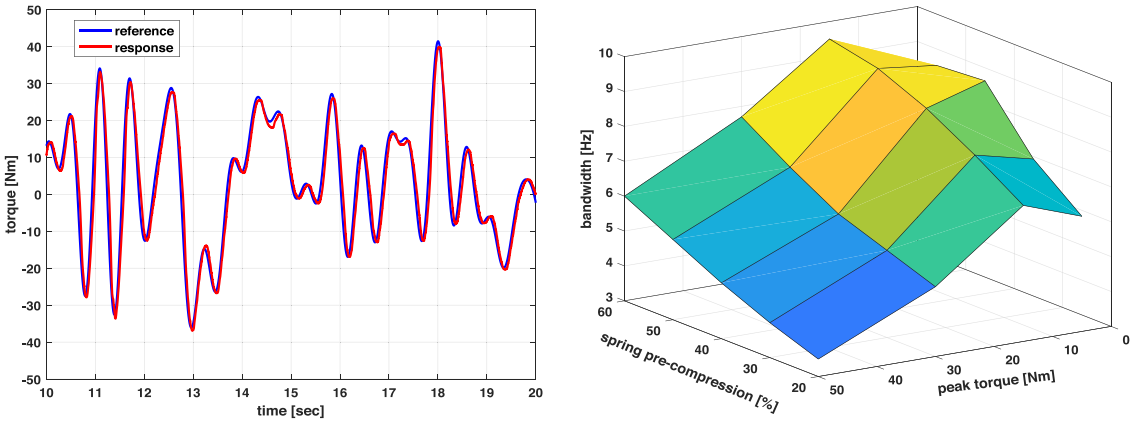


(a) MACCEPA's multi-sine response. (b) MACCEPA's bandwidth.

**Fig. 9.** The MACCEPA's response to a multi-sine torque reference trajectory, generated using a code written in Matlab. a) The output torque delivered while following an online-generated lever arm reference position closely matches the actual measured torque, confirming the validity of the torque and stiffness approximations. The test is done with 40% MACCEPA spring pre-compression, following a multi-sine signal with 2 Hz frequency spectrum. b) The actuator's bandwidth as a function of different MACCEPA spring pre-compression (20,30,40,50 and 60%) and a different peak torque (5,15,30 and 50 Nm). The results shown are for the fixed output angle $\theta_{BIO}$=40°. As expected, the bandwidth increases with the spring pre-compression and decreases with the peak torque. Slight alterations to this can be seen at a very low torque (5 Nm), which is likely due to the actuator's dead-zone around zero torque.

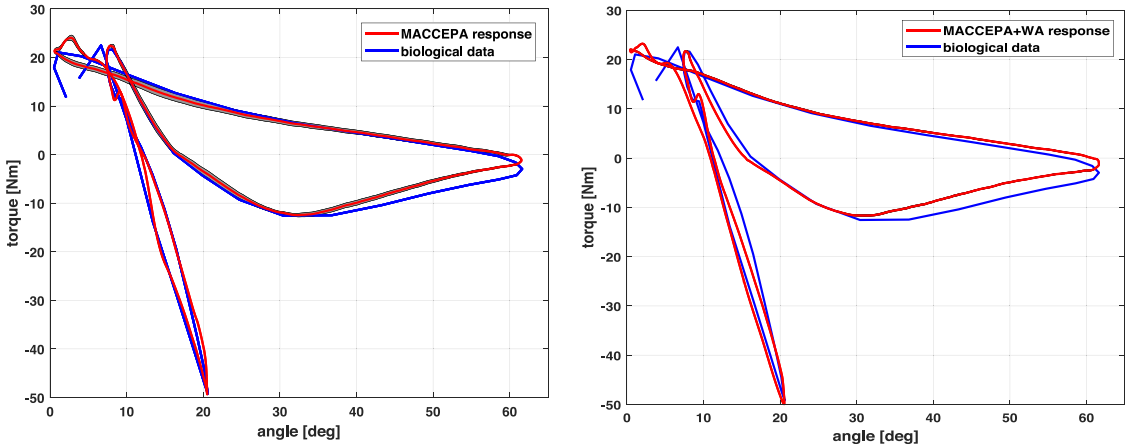


(a) Gait torque delivered by the MACCEPA. (b) Gait torque delivered by the MACCEPA+WA.

**Fig. 10.** Knee joint torque-angle characteristic of a healthy 80 kg human during 4.7 km/h walking [33] stretched to 2.3 s/stride due to the MACCEPA's motor speed limitation. The data is calculated as an average over 50 gait cycles. Small standard deviation (SD, shaded area around mean trajectory) shows that the actuator's response is highly repeatable and robust. The MACCEPA's spring was pre-compressed to 40%. a) The MACCEPA can deliver the entire gait cycle but that comes at a cost of a high peak power during the WA phase. The discrepancy seen around the peak knee flexion comes from the MACCEPA's lower accuracy at low torques, especially when the torque sign changes. b) During the WA phase, the MACCEPA is in zero-torque mode. As expected, the WA mechanism has an almost linear output characteristic, which matches the biological joint quasi-stiffness. The WA mechanism is engaged at the biological angle corresponding to zero biological torque due to its unilateral torque output.

### *6.2. Dynamic benchmarking*

During dynamic benchmarking, the actuator was tested in two modes. In the first mode, the MACCEPA unit alone is delivering the knee joint torque during the entire gait cycle. In the second mode, both SEA and PEA units are delivering the torque throughout the gait cycle. Since the actuator's output link is actively controlled by the load motor, all the tests are performed using an open-loop torque controller in series to the MACCEPA's lever arm closed-loop position control. The load motor's setpoint is the biological knee joint angle (Winter walking data [33] at 4.7 km/h stretched to a 2.3 s/stride), while the biological knee joint torque from the same dataset is used as the actuator's setpoint. All references are time-dependent.

Fig. 10 shows the actuator's output torque during the entire gait cycle, when the MACCEPA alone is used to deliver the desired output (Fig. 10a) and when the MACCEPA and WA mechanism are both working throughout the gait cycle (Fig. 10b). Although the output was delivered without the controller having any knowledge of the actual torque, due to the accuracy of

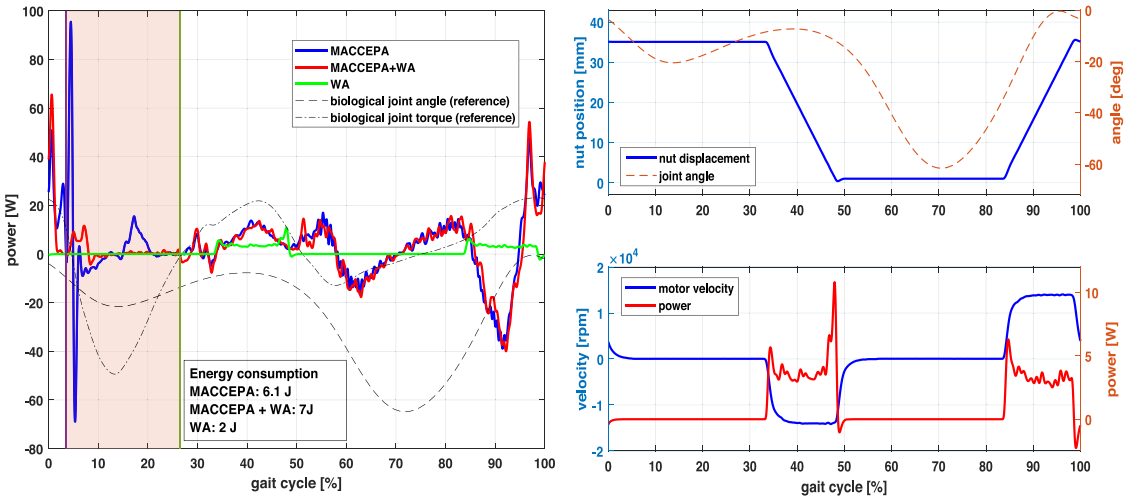


(a) Actuator power throughout gait cycle. (b) WA mechanism power and nut motion.

**Fig. 11.** The whole actuator electrical power consumption during the gait cycle. The data is calculated as an average over 50 gait cycles (SD not shown due to its very small and bare visibility). a) Engaging the WA mechanism during the early stance phase (brown shaded area) significantly offloads the MACCEPA. The power peak seen at the very end and beginning of the cycle comes from the nature of the used torque reference data. b) The nut is moved to its engagement position just before the weight bearing starts (84–98% of the gait cycle) and then to its lowest position once the WA is finished (34–48% of the gait cycle), thus allowing the leg to swing freely. As seen in the upper figure, the nut is engaged from 7% to 25% of the gait cycle (i.e. when the biological angle trajectory is below the nut position trajectory). When the nut is not moving, the motor driver is switched off to avoid energy loss coming from the drive. The WA mechanism's average power consumption is 0.86 W per gait cycle.

torque and stiffness approximations, the MACCEPA is a reliable torque source. During the early stance phase when the WA mechanism is engaged, the MACCEPA can either work in a zero-torque mode, as is the case here, or in the superimposing mode. In the latter case, the MACCEPA can add to or subtract energy from the system simultaneously with the WA torque that is passively delivered by the WA mechanism. This is useful when the WA angular stiffness does not match the biological joint quasi-stiffness. The effect of such an approach will be the subject of a future study.

The WA mechanism is added to the MACCEPA unit in order to decrease its power peaks and energy consumption by offloading its motor during the early stance phase. Fig. 11a provides comparison of the motor electrical power consumption of the actuator in MACCEPA-only mode and MACCEPA+WA mode. As seen, the MACCEPA's peak power during the early stance phase is reduced by an order of magnitude and its average power consumption over the gait cycle from 2.66 W to 2.17 W (20%) when the WA mechanism is engaged. Given that the WA mechanism's angular stiffness corresponds to a biological knee joint quasi stiffness (see Fig. 10b), the MACCEPA is in zero-torque mode during the early stance gait phase. The WA mechanism reaches a peak electrical motor power of around 10 W when the nut is moved to its (dis)engagement position, resulting in about 2 J of electrical energy per stride. This is around five times less than the similar mechanism in [23] due to a lower motor velocity and smaller mass moving along the spindle. Although an engagement of the WA mechanism did reduce the MACCEPA's energy consumption for about 1 J, the total actuator energy increased 1 J when compared to the MACCEPA only. This is because the total energy balance of the actuator comes to a large extent from accelerations and deccelerations of the inertia during the swing phase.

## 7. Discussion and conclusions

Being able to fully and efficiently replicate biologically relevant joint kinetics and kinematics is vital for assistance and rehabilitation tasks in cases where orthotic devices need to adjust to the user wearing them. The actuation unit's design for such WRs needs to be approached from two different angles: the user's point of view and the actuator's point of view. Although these may sometimes lead to opposing and conflicting requirements, there exists a common ground that WRs should be built upon: wearability, efficiency, adaptability, and, most importantly, safety.

In this paper, we have presented the design and evaluation of a novel modular compliant knee joint actuator (Figs. 1 and 5) for use in a knee joint of a standalone and/or multi-joint lower-limb orthosis. The distinctive property of the actuator is a combination of two independent yet complementary compliant actuation units, built around parallel and series elasticity concepts (Fig. 3). By combining the two, the actuator takes advantages of both concepts, thus having the potential to efficiently exploit (via parallel elasticity) and fully mimic (via series elasticity) dynamic behavior of the knee joint during walking. Adding compliance to the actuation system inherently increases the safety of both the user and the actuator by increasing tolerance to impact loads. The benefit of having a system of variable output impedance, as is the case with the actuator presented herein, is the possibility to adjust to each user's biomechanics and individual therapeutic requirements.

**Table 1**
Comparison of physical VSA systems and their specifications.

| Actuator | Weight [kg] | Width [mm] | Peak $\tau$ [Nm] | $\tau$ density [Nm/kg] | $\kappa$ range [Nm/rad] | $\tau$ sensor embedded |
|---|---|---|---|---|---|---|
| VSA(+PEA)[1] | 1.15(1.5) | 58 | 70[2] | 60.9(46.6) | 0–487 | Yes |
| AwAS-II [13] | 1.1 | 140 | 80 | 72.7 | 0-Rigid | No |
| CompAct-VSA [12] | 1.8 | – | 117 | 65 | 0-Rigid | No |
| MACCEPA 2.0 [47] | 2.4 | – | 70 | 29.2 | 5–110 | Yes |
| MIRAD [48] | 1.4 | 112 | 15 | 10.7 | 28.5–86 | Yes |
| ARES [14] | 1.1 | 70 | 76 | 69.1 | 143–744 | Yes |
| ARES XL [49] | 1.2 | 70 | 76 | 63 | 0–860 | Yes |
| SVSA [7] | 2.4 | 85 | 60 | 25 | 5–110 | Yes |
| BAFSA [15] | 2.96 | 95 | 72 | 24.3 | – | – |

$\tau$ = torque; $\kappa$ = stiffness; [1]actuator presented herein; [2]reached with $\theta_{BIO}$=40° (see Fig. 3).

Since the actual benefits of changing the stiffness within a single activity have not yet been demonstrated, the actuator is designed to be able to change its stiffness offline, across different activities. Such an approach is also more relevant for a post-stroke patients, the target group of our work, for which it is more interesting to be able to change actuator's output stiffness across gait cycles, allowing stiff actuation in the early phases of their therapy (robot-in-charge mode) and a more compliant actuation in the late phases of their therapy (human-in-charge mode).

A series elasticity unit is built around the MACCEPA concept, previously successfully applied in orthotics and prosthetics owing to its simplicity. In the presented knee joint-specific actuator, the MACCEPA concept is realized as a spindle-driven VSA (Figs. 1 and 3). Due to the employment of a highly efficient, backdrivable spindle and low system friction, the actuator can deliver biological torque (Fig. 10a) with a relatively small electrical energy consumption per gait cycle (Fig. 11a). Although the knee joint mainly dissipates energy during the gait cycle, the presented MACCEPA stays on the positive side of energy balance, relatively close to zero, due to the inertial effects dominating the swing phase. This difference in energy balance indicates that there is a potential for further improving the actuator's energy efficiency. One possible way to achieve this could be through a reduction in the reflected load inertia by decreasing the total MACCEPA's gear ratio. However, it is not clear whether this would have any beneficial effect as lower gear ratio requires a higher torque motor which, in turn, not only has a higher rotor inertia but can also attain smaller output velocities. Furthermore, the goal of designing this actuator was not reaching the highest attainable absolute efficiency in the knee actuation unit but to show, in relative terms, the benefits of adding a quasi-passive mechanism working parallel to the main, active actuation unit which we argue is beneficial to have. This is because an active actuation unit during the stance and swing phase, unlike passive ones, allows accurate replication of biologically relevant knee joint kinetics and kinematics (as shown in Fig. 10a). Additionally, having an active unit as part of a knee joint actuator allows the use of the actuator in other ADLs as well.

In addition to benefiting the actuator's energy consumption and its orthosis' autonomy, linear actuator realization also has positive effects on the user. The actuator's lateral protrusion is only 58mm, the smallest of all SoA actuators reported in Table 1, and well below what users define as an obstacle in ADLs [14]. Furthermore, spindle-based design allowed improvements in mass and inertia distribution along the leg segments, which is important as mass is the main contributor to the increase in the metabolic cost of walking [35]. By including sensors and connections to the user but without the use of electronics and batteries, the MACCEPA weighs 1.15 kg. This, in combination with a maximum torque output of 70 Nm, makes the MACCEPA second only to ARES of all the VSAs applied in orthotics when it comes to torque-density. The MACCEPA does, however, use a 70 W motor to deliver such performance, unlike ARES and ARES XL, which use a 90 W motor.

Human leg joints perform both positive and negative work during locomotion, allowing more energy efficient actuation if part of that energy can be passively stored and reused. The gait's WA phase in the knee joint allows just that as it is energetically demanding [33] but behaves as a simple torsional spring [32]. Changes in gravitational potential energy of this gait phase are harvested using a simple, quasi-passive mechanism (Fig. 5) working parallel to the MACCEPA. When engaged, the mechanism drains no energy from the power source due to its non-backdrivable spindle providing a reactionary torque by friction-locking the nut (Fig. 11c). The device's small energetic cost comes from a small EC motor moving the nut, unloaded, to the engagement position once in every gait cycle. As it is quasi-passive, this mechanism cannot contribute positive mechanical energy to the system. However, its main function is only to complement VSA, a versatile active device that can both contribute mechanical energy in and dissipate it from the system. By doing so, as demonstrated in this paper, the VSA's peak power was reduced by an order of magnitude (see Fig. 11a). This means that, when used with the WA mechanism, the MACCEPA's 70W motor can be easily replaced by a lower power motor without compromising the actuator's output performance. In addition, the WA mechanism can be used as a fall-prevention mechanism during other ADLs by providing a high leg stiffness and extension torque to prevent the leg from collapsing.

Despite having an infinite locking resolution useful for several reasons [23], the WA mechanism's energy storing capacity depends on a resulting fixed spring constant. This is an important limitation as changes in human joint stiffness account for changes in people's weight, walking speed, and surface stiffness, among others. If the WA mechanism's angular stiffness corresponds to the desired biological joint quasi-stiffness (e.g. red line in Fig. 2), the action of engaging the WA spring at a proper angle will result in a desired torque-angle response (see Fig. 10b). However, if this is not the case, the engagement angle's choice becomes a trade-off between assisted torque and stable interaction with the user. Too high/low WA

mechanism's angular stiffness will result in either i) too high/low torque, if engaged at optimal angle or ii) too high/low engagement angle if the required torque is to be delivered. Thus, in both cases, the suboptimal spring stiffness is likely to lead to discomfort and instability while walking. One way to overcome the problem of the WA mechanism's fixed angular stiffness is to have the MACCEPA working together with the WA mechanism during the early stance phase (i.e. superimposing the WA mechanism). This way, the actuator's angular stiffness during the early stance phase can be altered while having the WA mechanism still deliver most of the torque. This approach and its effects are going to be explored in the upcoming tests.

In the tests presented herein, the MACCEPA was in a zero-torque mode during the early stance phase as the WA mechanism's spring choice resulted in an optimal angular stiffness for a given torque-angle data (coming from [33]). Although the Winter walking data does not capture all the variability present in the humans' gait cycle, it does represent a typical gait pattern, making it a useful guideline in the actuator's design. In order to operate in a zero-torque mode during the early stance phase or to superimpose the WA mechanism, the MACCEPA's controller needs to be able to change its output depending on the output coming from the WA mechanism. To do so, the new low-level torque controller, built around an experimentally-based closed-form solution to the inverse MACCEPA equation, was developed and presented herein. The controller allows torque reference to be generated and delivered in real time without any information on the actuator's output torque due to model approximations that accurately capture the MACCEPA's dynamics (see Fig. 6). Being a reliable torque source without a torque sensor in the loop is one of the main advantages of the presented actuator since this sensor can, depending on its implementation, negatively affect actuator's weight, complexity, robustness and compactness. Another benefit of the presented controller is that it allows real-time stiffness control implementation, should that be required. In the current implementation, the MACCEPA's stiffness is changed offline by means of a simple keyed worm-gear mechanism. However, due to a stiffening effect, its stiffness is never a constant, but changes non-linearly with the deflection angle, as shown in Fig. 6b.

The goal of the upcoming work is to test the hypothesis that the actuator's energetic performance in delivering gait using both the MACCEPA and WA mechanism is positively correlated with a decrease in its angular stiffness. These tests will also show the effect of suboptimal WA mechanism's angular stiffness on the overall system's energetic performance when the MACCEPA needs to work against the WA mechanism in order to deliver desired torque-angle behavior. As an extension to the actuator bandwidth tests presented herein, the actuator's bandwidth will be tested in a different load inertia settings. This work in dynamic benchmarking environment will then be followed by the implementation of the actuator into the knee joint orthosis, which will allow studying the effect its variable compliance has on healthy and impaired users during different ADLs. It will also allow studying the effects of the actuator on the user's kinematics, kinetics, and biomechanics as well as the effect that the interface to the user has on the actuator's energetic performance and bandwidth.

## 8. Conflict of interest

The authors declare no conflict of interest.

## Acknowledgments

The presented work was developed within the projects BioMot (EC's 7th Framework Program, Grant Agreement number IFP7-ICT-2013-10-611695) and MIRAD (Flemish agency for Innovation by Science and Technology, IWT-SBO 120057) and it is partially supported by Flanders Make.

## References

[1] H. Geyer, A. Seyfarth, R. Blickhan, Compliant leg behaviour explains basic dynamics of walking and running, 2006. doi:10.1098/rspb.2006.3637.
[2] G.A. Pratt, M.M. Williamson, Series elastic actuators, Int. Conf. Intell. Robot. Syst. 1 (1995) 399–406.
[3] S. Wang, C. Meijneke, H. van der Kooij, Modeling, design, and optimization of mindwalker series elastic joint, in: 13th IEEE Int. Conf. Rehabil. Robot., 2013, pp. 1–8, doi:10.1109/ICORR.2013.6650381.
[4] H.K. Kwa, J.H. Noorden, M. Missel, T. Craig, J.E. Pratt, P.D. Neuhaus, Development of the IHMC mobility assist exoskeleton, in: Int. Conf. Robot. Autom., 2009, pp. 2556–2562, doi:10.1109/ROBOT.2009.5152394.
[5] L. Saccares, I. Sarakoglou, N.G. Tsagarakis, iT-Knee: an exoskeleton with ideal torque transmission interface for ergonomic power augmentation, in: IEEE/RSJ Int. Conf. Intell. Robot. Syst., 2016, pp. 780–786, doi:10.1109/IROS.2016.7759140.
[6] J.F. Veneman, R. Ekkelenkamp, R. Kruidhof, F.C.T. van der Helm, H. van der Kooij, Design of a series elastic- and Bowden cable-based actuation system for use as torque-actuator in exoskeleton-type training, in: Proc. 2005 IEEE, 2005, pp. 496–499, doi:10.1109/ICORR.2005.1501150.
[7] V. Grosu, C. Rodriguez-Guerrero, S. Grosu, B. Vanderborght, D. Lefeber, Design of smart modular variable stiffness actuators for robotic-assistive devices, IEEE/ASME Trans. Mechatron. 22 (4) (2017) 1777–1785, doi:10.1109/TMECH.2017.2704665.
[8] G. Chen, P. Qi, Z. Guo, H. Yu, Mechanical design and evaluation of a compact portable knee-ankle-foot robot for gait rehabilitation, Mech. Mach. Theory 103 (2016) 51–64, doi:10.1016/j.mechmachtheory.2016.04.012.
[9] K. Kong, J. Bae, M. Tomizuka, A compact rotary series elastic actuator for human assistive systems, IEEE/ASME Trans. Mechatron. 17 (2) (2012) 288–297, doi:10.1109/TMECH.2010.2100046.
[10] B. Vanderborght, A. Albu-Schaeffer, A. Bicchi, E. Burdet, D. Caldwell, R. Carloni, M. Catalano, O. Eiberger, W. Friedl, G. Ganesh, M. Garabini, M. Grebenstein, G. Grioli, S. Haddadin, H. Hoppner, A. Jafari, M. Laffranchi, D. Lefeber, F. Petit, S. Stramigioli, N. Tsagarakis, M. Van Damme, R. Van Ham, L. Visser, S. Wolf, Variable impedance actuators: a review, Rob. Auton. Syst. 61 (12) (2013) 1601–1614, doi:10.1016/j.robot.2013.06.009.
[11] R.V. Ham, B. Vanderborght, M.V. Damme, B. Verrelst, D. Lefeber, MACCEPA, the mechanically adjustable compliance and controllable equilibrium position actuator: design and implementation in a biped robot, Rob. Auton. Syst. 55 (10) (2007) 761–768, doi:10.1016/j.robot.2007.03.001.
[12] N.G. Tsagarakis, I. Sardellitti, D.G. Caldwell, A new variable stiffness actuator (CompAct-VSA): design and modelling, in: IEEE/RSJ Int. Conf. Intell. Robot. Syst., 2011, pp. 378–383, doi:10.1109/IROS.2011.6095006.

[13] A. Jafari, N.G. Tsagarakis, D.G. Caldwell, AwAS-II: a new actuator with adjustable stiffness based on the novel principle of adaptable pivot point and variable lever ratio, in: IEEE Int. Conf. Robot. Autom., 2011, pp. 4638–4643, doi:10.1109/ICRA.2011.5979994.
[14] M. Cestari, D. Sanz-Merodio, J.C. Arevalo, E. Garcia, An adjustable compliant joint for lower-Limb exoskeletons, IEEE/ASME Trans. Mechatron. 20 (2) (2015) 889–898, doi:10.1109/TMECH.2014.2324036.
[15] R.R. Torrealba, S.B. Udelman, E.D. Fonseca-Rojas, Design of variable impedance actuator for knee joint of a portable human gait rehabilitation exoskeleton, Mech. Mach. Theory 116 (2017) 248–261, doi:10.1016/j.mechmachtheory.2017.05.024.
[16] T. Bacek, M. Moltedo, K. Langlois, G.A. Prieto, M.C. Sanchez-Villamañan, J. Gonzalez-Vargas, B. Vanderborght, D. Lefeber, J.C. Moreno, BioMot exoskeleton - towards a smart wearable robot for symbiotic human-robot interaction, in: Int. Conf. Rehabil. Robot., 2017, pp. 1666–1671, doi:10.1109/ICORR.2017.8009487.
[17] M. Moltedo, T. Bacek, K. Junius, B. Vanderborght, D. Lefeber, Mechanical design of a lightweight compliant and adaptable active ankle foot orthosis, in: 6th IEEE Int. Conf. Biomed. Robot. Biomechatronics, 2016, pp. 1224–1229, doi:10.1109/BIOROB.2016.7523798.
[18] L. Flynn, J. Geeroms, R. Jimenez-Fabian, B. Vanderborght, N. Vitiello, D. Lefeber, Ankle-knee prosthesis with active ankle and energy transfer: development of the CYBERLEGs alpha-Prosthesis, Rob. Auton. Syst. 73 (2015) 4–15, doi:10.1016/j.robot.2014.12.013.
[19] T. Verstraten, P. Beckerle, R. Furnémont, G. Mathijssen, B. Vanderborght, D. Lefeber, Series and parallel elastic actuation: impact of natural dynamics on power and energy consumption, Mech. Mach. Theory 102 (2016) 232–246, doi:10.1016/j.mechmachtheory.2016.04.004.
[20] A.M. Dollar, H. Herr, Design of a quasi-passive knee exoskeleton to assist running, in: IEEE/RSJ Int. Conf. Intell. Robot. Syst., 2008, pp. 747–754, doi:10.1109/IROS.2008.4651202.
[21] K. Shamaei, P.C. Napolitano, A.M. Dollar, Design and functional evaluation of a quasi-passive compliant stance control knee-ankle-foot orthosis, IEEE Trans. Neural Syst. Rehabil. Eng. 22 (2) (2014) 258–268, doi:10.1109/TNSRE.2014.2305664.
[22] G. Elliott, A. Marecki, H. Herr, Design of a clutch-spring knee exoskeleton for running, J. Med. Device. 8 (3) (2014) 31002–31011.
[23] J. Geeroms, L. Flynn, R. Jimenez-Fabian, B. Vanderborght, D. Lefeber, Design and energetic evaluation of a prosthetic knee joint actuator with a lockable parallel spring, Bioinspir. Biomim. 12 (2) (2017) 26002.
[24] E.J. Rouse, L.M. Mooney, H.M. Herr, Clutchable series-elastic actuator: implications for prosthetic knee design, Int. J. Rob. Res. 33 (13) (2014) 1611–1625, doi:10.1177/0278364914545673.
[25] P. Beyl, K. Knaepen, S. Duerinck, M. Van Damme, B. Vanderborght, R. Meeusen, D. Lefeber, Safe and compliant guidance by a powered knee exoskeleton for robot-assisted rehabilitation of gait, Adv. Robot. 25 (5) (2011) 513–535, doi:10.1163/016918611X558225.
[26] A.J. Young, D.P. Ferris, State of the art and future directions for lower limb robotic exoskeletons, IEEE Trans. Neural Syst. Rehabil. Eng. 25 (2) (2017) 171–182, doi:10.1109/TNSRE.2016.2521160.
[27] M.R. Tucker, J. Olivier, A. Pagel, H. Bleuler, M. Bouri, O. Lambercy, J.d.R. Millán, R. Riener, H. Vallery, R. Gassert, Control strategies for active lower extremity prosthetics and orthotics: a review, J. Neuroeng. Rehabil. 12 (1) (2015) 1, doi:10.1186/1743-0003-12-1.
[28] T. Yan, M. Cempini, C.M. Oddo, N. Vitiello, Review of assistive strategies in powered lower-limb orthoses and exoskeletons, Rob. Auton. Syst. 64 (2015) 120–136, doi:10.1016/j.robot.2014.09.032.
[29] J. Zhang, C.C. Cheah, S.H. Collins, Experimental comparison of torque control methods on an ankle exoskeleton during human walking, in: 2015 IEEE Int. Conf. Robot. Autom., 2015, pp. 5584–5589, doi:10.1109/ICRA.2015.7139980.
[30] T. Bacek, M. Moltedo, K. Langlois, C. Rodriguez-Guerrero, B. Vanderborght, D. Lefeber, A novel modular compliant knee joint actuator for use in assistive and rehabilitation orthoses, in: 2017 IEEE/RSJ Int. Conf. Intell. Robot. Syst., 2017, pp. 5812–5817, doi:10.1109/IROS.2017.8206472.
[31] S. Masouros, A. Bull, A. Amis, Biomechanics of the knee joint, Orthop. Trauma 24 (2) (2010) 84–91, doi:10.1016/j.mporth.2010.03.005.
[32] K. Shamaei, A.M. Dollar, On the mechanics of the knee during the stance phase of the gait, in: IEEE Int. Conf. Rehabil. Robot., 2011, pp. 1–7, doi:10.1109/ICORR.2011.5975478.
[33] D.A. Winter, The Biomechanics and Motor Control of Human Gait: Normal, Elderly and Pathological, University of Waterloo Press, 1991.
[34] C. Frigo, P. Crenna, L.M. Jensen, Moment-angle relationship at lower limb joints during human walking at different velocities, J. Electromyogr. Kinesiol. 6 (3) (1996) 177–190, doi:10.1016/1050-6411(96)00030-2.
[35] K. Shamaei, M. Cenciarini, A.A. Adams, K.N. Gregorczyk, J.M. Schiffman, A.M. Dollar, Biomechanical effects of stiffness in parallel with the knee joint during walking, IEEE Trans. Biomed. Eng. 62 (10) (2015) 2389–2401, doi:10.1109/TBME.2015.2428636.
[36] J. Zhang, S.H. Collins, The passive series stiffness that optimizes torque tracking for a lower-limb exoskeleton in human walking, Front. Neurorobot. 11 (2017) 68, doi:10.3389/fnbot.2017.00068.
[37] T. Bacek, R. Unal, M. Moltedo, K. Junius, H. Cuypers, B. Vanderborght, D. Lefeber, Conceptual design of a novel variable stiffness actuator for use in lower limb exoskeletons, in: IEEE Int. Conf. Rehabil. Robot., 2015, pp. 583–588, doi:10.1109/ICORR.2015.7281263.
[38] D. Zanotto, Y. Akiyama, P. Stegall, S.K. Agrawal, Knee joint misalignment in exoskeletons for the lower extremities: effects on user's gait, IEEE Trans. Robot. 31 (4) (2015) 978–987, doi:10.1109/TRO.2015.2450414.
[39] V. Bartenbach, Constraints caused by lower extremity exoskeletons, 2017 Ph.D. Thesis.
[40] A. Schiele, F.C.T. van der Helm, Kinematic design to improve ergonomics in human machine interaction, IEEE Trans. Neural Syst. Rehabil. Eng. 14 (4) (2006) 456–469, doi:10.1109/TNSRE.2006.881565.
[41] D. Wang, K.M. Lee, J. Guo, C.J. Yang, Adaptive knee joint exoskeleton based on biological geometries, IEEE/ASME Trans. Mechatron. 19 (4) (2014) 1268–1278, doi:10.1109/TMECH.2013.2278207.
[42] K. Langlois, M. Moltedo, T. Bacek, C. Rodriguez Guerrero, B. Vanderborght, D. Lefeber, Design and development of customized physical interfaces to reduce relative motion between the user and a powered ankle foot exoskeleton, in: IEEE Int. Conf. Biomed. Robot. Biomechatronics, Accept., 2018.
[43] M.K. Shepherd, E.J. Rouse, Design and validation of a torque-controllable knee exoskeleton for sit-to-Stand assistance, IEEE/ASME Trans. Mechatron. 22 (4) (2017) 1695–1704, doi:10.1109/TMECH.2017.2704521.
[44] T. Verstraten, J. Geeroms, G. Mathijssen, B. Convens, B. Vanderborght, D. Lefeber, Optimizing the power and energy consumption of powered prosthetic ankles with series and parallel elasticity, Mech. Mach. Theory 116 (2017) 419–432, doi:10.1016/j.mechmachtheory.2017.06.004.
[45] K. Langlois, T. van der Hoeven, D.R. Cianca, T. Verstraten, T. Bacek, B. Convens, C. Rodriguez-Guerrero, V. Grosu, D. Lefeber, B. Vanderborght, Ethercat tutorial: an introduction for real-time hardware communication on windows [Tutorial], IEEE Robot. Autom. Mag. 25 (1) (2018) 22–122, doi:10.1109/MRA.2017.2787224.
[46] J. Malzahn, N. Kashiri, W. Roozing, N. Tsagarakis, D. Caldwell, What is the torque bandwidth of this actuator? in: 2017 IEEE/RSJ Int. Conf. Intell. Robot. Syst., 2017, pp. 4762–4768, doi:10.1109/IROS.2017.8206351.
[47] B. Vanderborght, N.G. Tsagarakis, C. Semini, R.V. Ham, D.G. Caldwell, MACCEPA 2.0: adjustable compliant actuator with stiffening characteristic for energy efficient hopping, in: 2009 IEEE Int. Conf. Robot. Autom., 2009, pp. 544–549, doi:10.1109/ROBOT.2009.5152204.
[48] B. Brackx, J. Geeroms, J. Vantilt, V. Grosu, K. Junius, H. Cuypers, B. Vanderborght, D. Lefeber, Design of a modular add-on compliant actuator to convert an orthosis into an assistive exoskeleton, in: 5th IEEE RAS/EMBS Int. Conf. Biomed. Robot. Biomechatronics, 2014, pp. 485–490, doi:10.1109/BIOROB.2014.6913824.
[49] M. Cestari, D. Sanz-Merodio, E. Garcia, A new and versatile adjustable rigidity actuator with add-on locking mechanism (ARES-XL), 2018. doi:10.3390/act7010001.